Acta Crystallographica Section F
Structural Biology Communications
ISSN 2053-230X

Use of a novel microtitration protocol to obtain diffraction-quality crystals of 4-hydroxy-2-oxoglutarate aldolase from *Bos taurus*

Amadeus Huang, Edward Baker* and Kerry Loomes*

School of Biological Sciences and Maurice Wilkins Centre for Molecular Biodiscovery, University of Auckland, Auckland 1010, New Zealand

Correspondence e-mail: en.baker@auckland.ac.nz, k.loomes@auckland.ac.nz

Received 4 August 2014
Accepted 29 September 2014

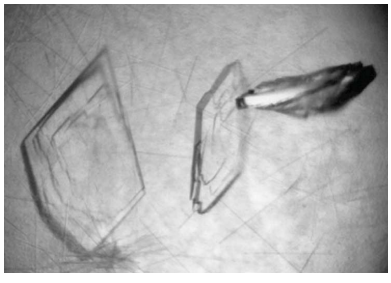

The enzyme 4-hydroxy-2-oxoglutarate aldolase (HOGA) catalyses the retro-aldol degradation of 4-hydroxy-2-oxoglutarate to pyruvate and glyoxylate as part of the hydroxyproline catabolic pathway in mammals. Mutations in the coding region of the human HOGA gene are associated with primary hyperoxaluria type 3, a disease characterized by excessive oxalate production and ultimately stone deposition. Native HOGA was purified from bovine kidney using an improved and streamlined purification protocol from which two crystal forms were obtained using two different approaches. Vapour diffusion using PEG 3350 as a precipitant produced monoclinic crystals that belonged to space group *C*2 and diffracted to 3.5 Å resolution. By comparison, orthorhombic crystals belonging to space group *I*222 or $I2_12_12_1$ and diffracting to beyond 2.25 Å resolution were obtained using a novel microtitration protocol with ammonium sulfate. The latter crystal form displayed superior diffraction quality and was suitable for structural determination by X-ray crystallography.

1. Introduction

4-Hydroxy-2-oxoglutarate aldolase (HOGA; EC 4.1.3.16) is a class I pyruvate-dependent aldolase located in the mitochondrial matrix of mammalian species. HOGA participates in the catabolic pathway for hydroxyproline degradation, where it catalyses the retro-aldol cleavage of the five-carbon intermediate 4-hydroxy-2-oxoglutarate to glyoxylate and pyruvate (Riedel *et al.*, 2011; Monico *et al.*, 2011). Mutations in the human gene coding for HOGA are associated with type 3 primary hyperoxaluria (PH3), a disease characterized by excessive endogenous production of oxalate, potentially leading to renal deposition of calcium oxalate crystals and renal failure (Belostotsky *et al.*, 2010). Studies using isotopically labelled metabolites have identified the glyoxylate product of HOGA as the primary source of endogenous oxalate synthesis (Jiang *et al.*, 2012; Takayama *et al.*, 2003). In order to design intervention strategies for PH3, it is necessary to understand the metabolic changes caused by HOGA mutations.

The crystal structure of human HOGA has been determined by X-ray crystallography and determined to be a homotetramer (Riedel *et al.*, 2011). The monomers are arranged in *D*2 symmetry, resembling the distantly related bacterial dihydrodipicolinate synthase enzymes (DHDPS) involved in lysine biosynthesis (Reboul *et al.*, 2012). The most prevalent pathogenic allele found in PH3 causes the in-frame deletion of Glu315. This residue is not directly involved in catalysis at the active site but instead is located in close proximity to the Glu313–Arg144′ salt bridge which stabilizes the major dimer interface (PDB entry 3s5n; Riedel *et al.*, 2011). For *Escherichia coli* DHDPS, disruption of the major dimer interface by mutations leads to increased protein aggregation and greatly reduced catalytic efficiency (Reboul *et al.*, 2012). It is therefore conceivable that deletion of residue Glu315 in the HOGA structure could weaken the dimer interface, leading to protein aggregation and loss of enzymatic function.

In the present study, we focused on the bovine isoform of HOGA, in which the Glu313–Arg144′ salt bridge is absent. The bovine enzyme has been successfully purified and characterized, but its molecular structure has not yet been reported (Riedel *et al.*, 2011; Dekker & Kitson, 1992). Interestingly, there is uncertainty as to

whether bovine HOGA actually exists as a dimer or a tetramer in solution (Kobes & Dekker, 1969, 1971), raising the possibility that tetramer formation may not be essential for catalysis. Determination of the bovine HOGA crystal structure might therefore offer new insights into the significance of the dimer interface in HOGA function and in the pathogenesis of PH3.

Here, we report an improved purification method of HOGA from bovine kidney tissue and a novel crystallization protocol combining batch and vapour-diffusion techniques. Using this modified protocol with ammonium sulfate as the sole precipitant, we obtained improved diffraction-quality crystals of sufficient quality to permit structural analysis of bovine HOGA.

2. Materials and methods

2.1. Macromolecule production

Purification of native HOGA from bovine kidneys was carried out using a protocol developed in-house based on previous reports (Riedel *et al.*, 2011; Dekker & Kitson, 1992). All purification steps were performed at 293 K unless otherwise mentioned. Mitochondria were purified from bovine kidney cortex by differential centrifugation in mannitol–sucrose buffer as described previously (Wieckowski *et al.*, 2009). Isolated mitochondria were resuspended in four volumes of PBS-EDTA (25 m*M* sodium phosphate pH 7.4, 150 m*M* NaCl, 1 m*M* EDTA) and lysed using a French press (Consonant Systems) operated at 18.5 kPa. The lysate was heated with agitation in a boiling water bath to 343 K and immediately cooled to 273 K in an ice–water slurry. The suspension was cleared by centrifugation (20 000*g*, 30 min) to remove denatured heat-labile components. Under these conditions, HOGA remains heat-stable and is active in the aqueous phase. Following the addition of solid ammonium sulfate to 30% saturation (180 mg ml^{-1}, 277 K) the mixture was stirred for 1 h followed by centrifugation (20 000*g*, 30 min).

The supernatant was loaded onto a hydrophobic interaction column (Phenyl Sepharose HP; GE Healthcare) pre-equilibrated with buffer *A* [1.2 *M* ammonium sulfate, 50 m*M* Tris–HCl pH 8.0, 0.5 m*M* tris(carboxyethyl)phosphine hydrochloride (TCEP)]. The column was washed with a series of step gradients of decreasing concentrations of ammonium sulfate. Bound bovine HOGA was eluted in buffer *A* without ammonium sulfate and identified by immunoblotting using an anti-HOGA polyclonal antibody (Sigma–Aldrich).

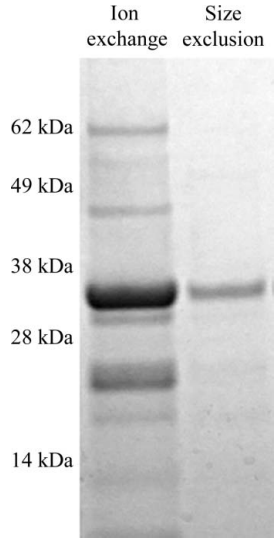

Figure 1
SDS–PAGE electrophoresis carried out under reducing conditions for bovine HOGA samples before and after size-exclusion chromatography. Purified bovine HOGA was resolved as a single band with an apparent molecular weight of 33 kDa.

Table 1
Crystallization.

	Form 1	Form 2
Method	Vapour diffusion	Vapour diffusion (microtitration)
Temperature (K)	291	291
Protein concentration (mg ml^{-1})	15	15
Buffer composition of protein solution	50 m*M* Tris–HCl pH 8.0, 150 m*M* NaCl, 0.5 m*M* TCEP	50 m*M* Tris–HCl pH 8.0, 150 m*M* NaCl, 0.5 m*M* TCEP
Composition of reservoir solution	100 m*M* HEPES–NaOH pH 7.0, 200 m*M* Na_2SO_4, 22.5% PEG 3350, 20% glycerol	100 m*M* Tris–HCl pH 8.0, 1.8 *M* ammonium sulfate
Volume and ratio of drop	2 µl, 1:1 (protein:reservoir)	Up to 6 µl (1 µl protein, 1 µl saturated ammonium sulfate, 1 µl storage buffer *B*, ≤3 µl water)
Volume of reservoir (ml)	1	1

The fraction containing HOGA was subsequently applied onto an anion-exchange column (Sepharose Q FF; GE Healthcare) pre-equilibrated with buffer *A* without ammonium sulfate. Bound proteins were eluted using a linear NaCl gradient from 0 to 400 m*M*. Fractions with the highest HOGA activity were identified using an LDH-coupled assay (Dekker & Kitson, 1992) and were then pooled and analysed by SDS–PAGE (Fig. 1, left lane). Solid ammonium sulfate was added to 40% saturation (240 mg ml^{-1}) to precipitate HOGA, which was pelleted by centrifugation (20 000*g*, 30 min) and re-solubilized in a minimal volume of deionized water. The concentrated protein solution was applied onto a size-exclusion column (Superdex 200 10 × 300 mm; GE Healthcare) pre-equilibrated with buffer *B* (50 m*M* Tris–HCl pH 8.0, 150 m*M* NaCl, 0.5 m*M* TCEP) and eluted at 0.3 ml min^{-1}. Bovine HOGA eluted with a retention position consistent with a 90 kDa globular protein and was essentially pure as analysed by SDS–PAGE (Fig. 1, right lane). This retention position is likely to correspond to the tetrameric form, as the human HOGA isoform also displays the same elution profile but nevertheless exists as a 120 kDa tetrameric species in the crystal structure (Riedel *et al.*, 2011). Fractions containing pure HOGA were identified by SDS–PAGE, concentrated to 15 mg ml^{-1} by ultrafiltration (3000*g*, 30 kDa MWCO Vivaspin Concentrator, GE Healthcare) and stored in liquid nitrogen. A kilogram of whole bovine kidney containing approximately 400 g of cortical tissue typically yielded 1 mg of purified HOGA.

ESI-MS analysis of purified bovine HOGA revealed two major m/z peaks consistent with the theoretical mass of residues 23–327 (32 553.4 Da) or 22–327 (32 709.2 Da) of the full-length bovine HOGA pro-peptide (UniProt Accession Q0P5I5). There was no evidence of post-translational modifications.

2.2. Crystallization

Initial screening was performed using a custom-designed 24-condition sparse-matrix screen based on a series of conditions reported in the literature for crystallizing human HOGA and other structurally related DHDPS/NAL superfamily enzymes (Kefala *et al.*, 2008; Evans *et al.*, 2011; Bunker *et al.*, 2012; Hendry *et al.*, 2000). Vapour-diffusion experiments were set up in 24-well VDX plates as

hanging drops at 291 K. One condition (100 m*M* HEPES–NaOH pH 7.0, 200 m*M* ammonium sulfate, 22.5% PEG 3350, 20% glycerol) yielded fine needles as well as large stacked plates (form 1) which grew to maximum dimensions of 0.5 × 0.4 × 0.05 mm over 2–3 weeks (Fig. 2*a*).

Another crystal form was obtained using a novel microtitration method adapted from previous reports (Spurlino *et al.*, 1994; Botos *et al.*, 1999). Under the view of a stereo microscope, 1 µl saturated ammonium sulfate solution (744 mg ml^{-1}) was added to a 1 µl drop of protein solution. Following the formation of an amorphous precipitate, 1 µl buffer *B* was added. The suspension was thoroughly mixed by pipetting and deionized water was then added in 0.5 µl increments to a maximum of 3 µl with mixing until the precipitate was no longer visible under dark-field illumination. The mixture was subsequently equilibrated as hanging drops at 291 K against 1 ml reservoir solution (100 m*M* Tris–HCl pH 8.0, 1.8 *M* ammonium sulfate). Rod-like crystals (form 2) appeared within 24 h; one crystal grew to 0.3 mm in the longest dimension and was used subsequently for X-ray analysis (Fig. 2*b*). A summary of the crystallization conditions is shown in Table 1.

2.3. Data collection and processing

X-ray diffraction data were collected using Cu *Kα* radiation from a Rigaku MicroMax-007 HF equipped with MAR345 DTB image-plate detectors (MAR Technologies) and a 110 K cryostream (Oxford Cryosystems). Form 1 crystals were harvested and cooled directly in the cryostream. Form 2 crystals were soaked in a cryoprotectant solution (100 m*M* Tris–HCl pH 8.0, 1.6 *M* ammonium sulfate, 25% glycerol) for 90 s before flash-cooling in liquid nitrogen. Diffraction images were integrated using *XDS* (Kabsch, 2010). Scaling and merging were performed using *SCALA* (Evans, 2011).

Table 2
Data collection and processing.

Values in parentheses are for the outer shell.

	Form 1	Form 2
Diffraction source	Cu *Kα* anode	Cu *Kα* anode
Wavelength (Å)	1.5417	1.5417
Temperature (K)	110	110
Detector	MAR345	MAR345
Crystal-to-detector distance (mm)	300	200
Rotation range per image (°)	0.5	0.5
Total rotation range (°)	180	360
Exposure time per image (s)	600	600
Space group	*C*2	*I*222 or $I2_12_12_1$
Unit-cell parameters (Å, °)	*a* = 272.4, *b* = 78.07, *c* = 197.0, *α* = 90, *β* = 93.75, *γ* = 90	*a* = 92.74, *b* = 210.8, *c* = 348.6, *α* = *β* = *γ* = 90
Mosaicity (°)	1.3	0.27
Resolution range (Å)	82.22–3.50 (3.61–3.50)	90.19–2.25 (2.29–2.25)
Total No. of reflections	187173 (15322)	2405936 (116506)
No. of unique reflections	52130 (4457)	161505 (7925)
Completeness (%)	99.2 (98.6)	100.0 (100.0)
Multiplicity	3.6 (3.4)	14.9 (14.7)
$\langle I/\sigma(I)\rangle$	5.2 (2.1)	13.3 (3.0)
$R_{\rm r.i.m.}$	0.237 (0.629)	0.242 (1.194)
Overall *B* factor from Wilson plot (Å^2)	50.77	23.11

3. Results and discussion

Bovine kidney HOGA was purified to homogeneity from native tissue using an optimized protocol. The purified protein was resolved as a single band by SDS–PAGE and deemed suitable for crystallization (Fig. 1). Large plate-like crystals were obtained using PEG 3350 as a precipitant at 291 K (Fig. 2*a*). Flash-cooled crystals showed anisotropic diffraction to 3.3 Å resolution in the most favourable direction with high mosaicity. A complete data set was collected to 3.5 Å resolution. The crystals are most likely to belong to the monoclinic space group *C*2, with unit-cell parameters *a* = 272.4, *b* = 78.07, *c* = 197.0 Å, *β* = 93.75°; however, the indexing process was unstable and inconsistent between crystals. Visual inspection of diffraction images revealed many split spots indicative of multiple lattices within the crystal. Attempts to physically separate the fused plates were unsuccessful and attempts to alter the crystal morphology by various methods including fine screening, replicating the experiments at 277 K and additive screening (Additive Screen HT, Hampton Research) did not yield better diffracting crystals.

Historically, batch crystallization utilizing ammonium sulfate titration has been employed occasionally as a method to purify proteins from complex mixtures (Fisher, 1985). More recently, titration with ammonium sulfate was shown to be capable of generating diffraction-quality crystals for proteins that could not be crystallized otherwise (Botos *et al.*, 1999). Nevertheless, this method has not been widely reported owing to the relatively large working volumes involved and protracted incubation periods, which are most likely due to the slow rate of evaporation. To address these shortcomings, we developed a novel adaptation of the titration method referred to as 'microtitration' featuring a miniaturization of the working volume to less than 10 µl as well as a controlled rate of evaporation by utilizing a large reservoir.

Using this microtitration protocol, orthorhombic crystals of sufficient diffraction quality were obtained that belonged to space group *I*222 or $I2_12_12_1$, with unit-cell parameters *a* = 92.74, *b* = 210.8, *c* = 348.6 Å (Fig. 2*b*). Eight HOGA monomers in the asymmetric unit would give a Matthews coefficient ($V_{\rm M}$) of 3.26 Å^3 Da^{-1} and a solvent

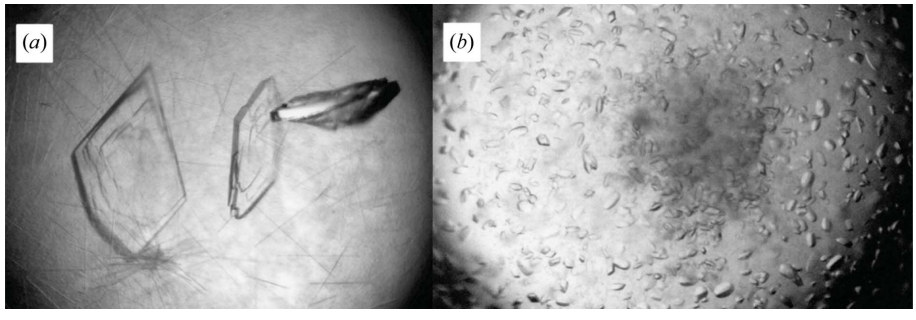

Figure 2
Bovine HOGA crystals. (*a*) Optimized form 1 crystals obtained using vapour diffusion showing closely fused plates that could not be separated without breakage. (*b*) Rod-like form 2 crystals using the microtitration method.

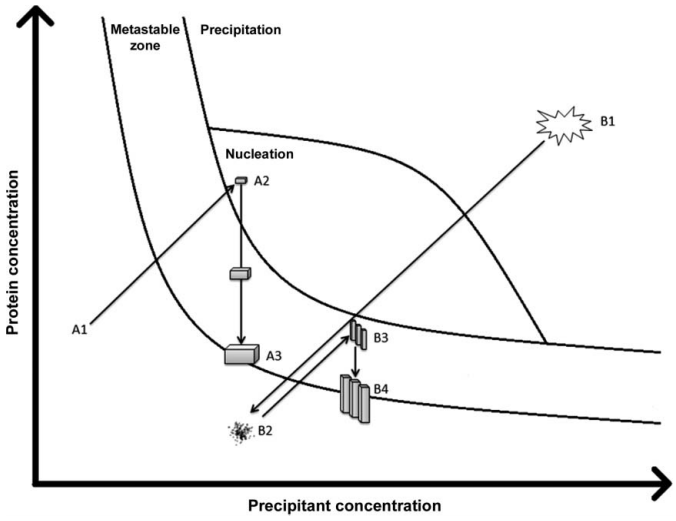

Figure 3
Phase diagram schematically summarizing putative events occurring during vapour diffusion (A1–A3) and microtitration methods (B1–B4) (Rupp, 2010; Chayen & Saridakis, 2008). With the vapour-diffusion method, an undersaturated solution is formed initially when the protein drop is mixed with the reservoir buffer (A1). Vapour diffusion against the more concentrated reservoir subsequently leads to supersaturation of the drop and initial crystal formation in the nucleation zone (A2). Crystal growth continues in the supersaturated metastable zone until the protein concentration in the surrounding environment falls below the solubility limit (A3). With the microtitration method the majority of protein precipitates when saturated ammonium sulfate solution is added to the drop (B1). The addition of water lowers the concentration of both protein and precipitant to the undersaturated region below the solubility curve; however, some precipitates persist (B2). The biphasic mixture is rapidly concentrated through vapour diffusion (B3). Once in the metastable zone, the persisting precipitates can act as nucleation centres to trigger crystal formation (B4).

content of 62% (Matthews, 1968). This could mean the presence of two tetramers or four dimers, but structural analysis will be required to resolve this question. The large unit-cell size, particularly along the extended *c* axis, resulted in spots that were difficult to resolve on our in-house X-ray diffraction facility. Nevertheless, an initial data set was collected that was complete to a resolution of 2.25 Å. Higher resolution is likely to be attainable using a synchrotron source.

It is worth noting that conditions with similar pH and ammonium sulfate concentrations were present in the initial vapour-diffusion screen, yet no crystals were produced. We postulate that some of the protein precipitates that formed initially upon addition of saturated ammonium sulfate did not redissolve during the titration process, thereby acting as nucleation centres for crystal growth (Fig. 3). The typical occurrence of small crystals observed through the microtitration protocol is consistent with this possibility. A potential variation of this protocol would be to remove these putative nucleation 'seeds' by filtration or centrifugation, which could result in fewer, larger crystals or possibly even abolish crystal formation. We did not test this possibility, however, as sufficient crystals of reasonable size were obtained using our existing protocol.

The diffraction characteristics for both crystal forms are summarized in Table 2. Overall, form 2 crystals obtained through the microtitration protocol exhibited favourable diffraction parameters compared with the form 1 crystals obtained using the hanging-drop method. Further refinements to improve reproducibility may include constituting a master mix prior to dispensing the drops. This microtitration crystallization protocol used to obtain bovine HOGA crystals might be applicable to other proteins which do not form diffraction-quality crystals using other methods.

This research was funded by the Maurice Wilkins Centre for Molecular Biodiscovery. We are grateful to Dr Christopher Squire and Dr Genevieve Evans for their assistance during data collection and processing. We also thank Martin Middleditch for carrying out the mass-spectrometric analysis of the protein samples.

References

Belostotsky, R., Seboun, E., Idelson, G. H., Milliner, D. S., Becker-Cohen, R., Rinat, C., Monico, C. G., Feinstein, S., Ben-Shalom, E., Magen, D., Weissman, I., Charon, C. & Frishberg, Y. (2010). *Am. J. Hum. Genet.* **87**, 392–399.
Botos, I., Meyer, E., Swanson, S. M., Lemaître, V., Eeckhout, Y. & Meyer, E. F. (1999). *J. Mol. Biol.* **292**, 837–844.
Bunker, R. D., Loomes, K. M. & Baker, E. N. (2012). *Acta Cryst.* F**68**, 59–62.
Chayen, N. E. & Saridakis, E. (2008). *Nature Methods*, **5**, 147–153.
Dekker, E. E. & Kitson, R. P. (1992). *J. Biol. Chem.* **267**, 10507–10514.
Evans, P. R. (2011). *Acta Cryst.* D**67**, 282–292.
Evans, G., Schuldt, L., Griffin, M. D. W., Devenish, S. R. A., Pearce, F. G., Perugini, M. A., Dobson, R. C. J., Jameson, G. B., Weiss, M. S. & Gerrard, J. A. (2011). *Arch. Biochem. Biophys.* **512**, 154–159.
Fisher, H. F. (1985). *Methods Enzymol.* **113**, 16–27.
Hendry, E. J., Buchanan, C. L., Russell, R. J. M., Hough, D. W., Reeve, C. D., Danson, M. J. & Taylor, G. L. (2000). *Acta Cryst.* D**56**, 1437–1439.
Jiang, J., Johnson, L. C., Knight, J., Callahan, M. F., Riedel, T. J., Holmes, R. P. & Lowther, W. T. (2012). *Am. J. Physiol. Gastrointest. Liver Physiol.* **302**, G637–G643.
Kabsch, W. (2010). *Acta Cryst.* D**66**, 125–132.
Kefala, G., Evans, G. L., Griffin, M. D. W., Devenish, S. R. A., Pearce, F. G., Perugini, M. A., Gerrard, J. A., Weiss, M. S. & Dobson, R. C. (2008). *Biochem. J.* **411**, 351–360.
Kobes, R. D. & Dekker, E. E. (1969). *J. Biol. Chem.* **244**, 1919–1925.
Kobes, R. D. & Dekker, E. E. (1971). *Biochim. Biophys. Acta*, **250**, 238–250.
Matthews, B. W. (1968). *J. Mol. Biol.* **33**, 491–497.
Monico, C. G., Rossetti, S., Belostotsky, R., Cogal, A. G., Herges, R. M., Seide, B. M., Olson, J. B., Bergstrahl, E. J., Williams, H. J., Haley, W. E., Frishberg, Y. & Milliner, D. S. (2011). *Clin. J. Am. Soc. Nephrol.* **6**, 2289–2295.
Reboul, C. F., Porebski, B. T., Griffin, M. D. W., Dobson, R. C. J., Perugini, M. A., Gerrard, J. A. & Buckle, A. M. (2012). *PLoS Comput. Biol.* **8**, e1002537.
Riedel, T. J., Johnson, L. C., Knight, J., Hantgan, R. R., Holmes, R. P. & Lowther, W. T. (2011). *PLoS One*, **6**, e26021.
Rupp, B. (2010). *Biomolecular Crystallography: Principles, Practice and Application to Structural Biology.* New York: Garland Science.
Spurlino, J. C., Smallwood, A. M., Carlton, D. D., Banks, T. M., Vavra, K. J., Johnson, J. S., Cook, E. R., Falvo, J., Wahl, R. C., Pulvino, T. A., Wendoloski, J. J. & Smith, D. L. (1994). *Proteins*, **19**, 98–109.
Takayama, T., Fujita, K., Suzuki, K., Sakaguchi, M., Fujie, M., Nagai, E., Watanabe, S., Ichiyama, A. & Ogawa, Y. (2003). *J. Am. Soc. Nephrol.* **14**, 939–946.
Wieckowski, M. R., Giorgi, C., Lebiedzinska, M., Duszynski, J. & Pinton, P. (2009). *Nature Protoc.* **4**, 1582–1590.